ORIGINAL RESEARCH

Phosphorylated cellulose nanofibers exhibit exceptional capacity for uranium capture

Janika Lehtonen · Jukka Hassinen · Avula Anil Kumar · Leena-Sisko Johansson ·
Roni Mäenpää · Nikolaos Pahimanolis · Thalappil Pradeep · Olli Ikkala ·
Orlando J. Rojas

Abstract We investigate the adsorption of hexavalent uranium, U(VI), on phosphorylated cellulose nanofibers (PHO-CNF) and compare the results with those for native and TEMPO-oxidized nanocelluloses. Batch adsorption experiments in aqueous media show that PHO-CNF is highly efficient in removing U(VI) in the pH range between 3 and 6. Gelling of nanofiber hydrogels is observed at U(VI) concentration of 500 mg/L. Structural changes in the nanofiber network (scanning and transmission electron microscopies) and the surface chemical composition (X-ray photoelectron spectroscopy) gave insights on the mechanism of adsorption. The results from batch adsorption experiments are fitted to Langmuir, Freundlich, and Sips isotherm models, which indicate a maximum adsorption capacity of 1550 mg/g, the highest value reported so far for any bioadsorbent. Compared to other metals (Zn, Mn, and Cu) and typical ions present in natural aqueous matrices the phosphorylated nanofibers are shown to be remarkably selective to U(VI). The results suggest a solution for the capture of uranium, which is of interest given its health and toxic impacts when present in aqueous matrices.

Keywords Cellulose nanofibers · Phosphorylated · Uranium · U(VI) · Adsorption · Heavy metal

J. Lehtonen · J. Hassinen (✉) · L.-S. Johansson ·
O. J. Rojas (✉)
Department of Bioproducts and Biosystems, School of Chemical Engineering, Aalto University, P.O. Box 16300, 00076 Aalto, Espoo, Finland
e-mail: jukka.hassinen@aalto.fi

O. J. Rojas
e-mail: orlando.rojas@aalto.fi

J. Hassinen · R. Mäenpää · O. Ikkala
Department of Applied Physics, School of Science, Aalto University, P.O. Box 16300, 00076 Aalto, Espoo, Finland

A. A. Kumar · T. Pradeep
DST Unit of Nanoscience (DST UNS) and Thematic Unit of Excellence (TUE), Department of Chemistry, Indian Institute of Technology Madras, Chennai 600036, India

N. Pahimanolis
Betulium Ltd., Tekniikantie 2, 02150 Espoo, Finland

O. J. Rojas
Departments of Chemical and Biological Engineering, Chemistry and Wood Science, The University of British Columbia, 2360 East Mall, Vancouver, BC V6T 1Z3, Canada

Introduction

Cellulose has been considered in the development of eco-friendly materials. Particularly, cellulose nanofibers (CNF) have raised interest for their suitability for water purification and heavy metal removal (Voisin et al. 2017). Chemical pretreatments have been used to reduce the energy consumed in CNF production and to introduce functional groups and charges on its surface. Such pretreatments include TEMPO oxidation, sulfonation, cationization, and phosphorylation (Klemm et al. 2018). The nanoscopic dimensions of CNF result in materials with a high surface area, which enhances interaction with metal ions (Bethke et al. 2018). Consequently, anionic CNF has been studied for removal of several heavy metals (Ma et al. 2012; Liu et al. 2015a). In this application, uranium is highly relevant given its occurrence in natural water as a result of leaching from mineral deposits and industrial processes, e.g., mining waters and nuclear fuel cycle facilities (WHO 2011; Kapnisti et al. 2018). In Finland, for example, concentrations as high as $\sim$ 15 mg/L have been determined for uranium in water obtained from drilled wells (Asikainen and Kahlos 1979). Uranium removal from these waters is important since it is both hazardous to the environment and toxic to humans. It can cause a kidney failure due to its chemical toxicity, which is typically of greater concern compared to its radioactivity (Kapnisti et al. 2018).

In aqueous media, two stable oxidation states are common for uranium, U(IV) and U(VI) (Aly and Hamza 2013; Xie et al. 2019). Under aerobic conditions, uranium is present in aqueous solutions in its hexavalent form as uranyl ions (UO_2^{2+}) (Sylwester et al. 2000; Cai et al. 2017; Sarafraz et al. 2017), which predominate in acidic environments (Riegel and Schlitt 2017). As pH increases, hydrolysis of uranyl leads to the formation of $(UO_2)_p(OH)_q^{(2p-q)}$ species (Berto et al. 2012). The uranyl ion can also form various complexes with carbonates present in groundwater (Xie et al. 2019). Due to uranyl complexation, in this manuscript U(VI) is discussed instead of UO_2^{2+} since we consider conditions where various UO_2^{2+} complexes are present.

The presented information points to the urgent need of technologies that are effective for uranium removal or to prevent the release of toxic concentrations of uranium into the environment (Ghasemi Torkabad et al. 2017). Common techniques used for heavy metal extraction include membrane processes, ion exchange, adsorption, precipitation, and solvent extraction (Chen et al. 2017; Xue et al. 2017; Sarafraz et al. 2017). As a low-cost, easily applicable alternative, adsorption has been considered promising for the removal of U(VI) from aqueous solutions (Su et al. 2018). In such application, bioadsorbents are sought after given a number of advantages including costs, geographical availability and the possibility of metal recovery after incineration.

Due to the high affinity of phosphoryl groups to uranium (Zhou et al. 2015), phosphorylated materials such as lignin (Bykov and Ershov 2009), pine wood sawdust (Zhou et al. 2015), graphene oxide (Liu et al. 2015b; Chen et al. 2017), carbon spheres (Yu et al. 2014), chitosan (Sakaguchi et al. 1981; Morsy 2015), cactus fibers (Prodromou and Pashalidis 2013), polyethylene (Shao et al. 2017), zirconium (Um et al. 2007), and mesoporous silica (Sarafraz et al. 2017; Xue et al. 2017), have been demonstrated for uranium removal. Phosphorous-based functional groups act as chelating agents and thus favor binding of uranyl species (Xie et al. 2019). Phosphorylated cellulose nanomaterials have been studied for adsorption of Fe^{3+} (Božič et al. 2014), Cu^{2+}, and Ag^+ (Liu et al. 2015a). In addition, CNF bearing bisphosphonate has been shown to be efficient for vanadium removal (Sirviö et al. 2016) while phosphorylated CNF nanopapers have been prepared for the removal of copper (Mautner et al. 2016). The removal of U(VI) has been studied with TEMPO oxidized CNF (TO-CNF), which achieved an adsorption capacity of 167 mg/g (Ma et al. 2012), and with carboxycellulose nanofibers prepared by nitro-oxidation, presenting a maximum adsorption capacity of 1470 mg/g (Sharma et al. 2017). However, to the best of our knowledge, there are no reports on the removal of U(VI) using phosphorylated CNF (PHO-CNF), which is surprising given the prospects indicated for other metals in the earlier studies.

In addition to chemical chelation, surface sorption mechanisms occur at the solid–liquid interface, such as physisorption, complexation, ion exchange, and precipitation, all of which play a crucial role for uranium removal (Xie et al. 2019). In this work, we study the removal of uranium with PHO-CNF using several batch adsorption approaches. Furthermore, we compare the uranium removal efficiency of PHO-CNF

with different phosphorylation degrees with that determined for native CNF and TO-CNF. The nanocelluloses are characterized by Fourier transform infrared spectroscopy (FT-IR), zeta potential measurements, and transmission electron microscopy (TEM) imaging. Results from the scanning electron microscopy (SEM), TEM, and X-ray photoelectron spectroscopy (XPS) after adsorption are found to give insights into the adsorption mechanism of U(VI). The effect of pH on the adsorption of U(VI) and selectivity against other metals are also studied. Adsorption data at pH 6 are fitted to the Langmuir, Freundlich, and Sips isotherm models. The data was found to fit best with the Sips isotherm, demonstrating a maximum adsorption capacity of 1550 mg/g, the highest among the values reported so far for organic adsorbents.

Experimental

Materials

Native CNF was produced at Aalto University from bleached birch pulp by a method reported previously (Rajala et al. 2016). PHO-CNF and TO-CNF were obtained from Betulium Oy, Finland. The concentrations of phosphoryl groups provided by the manufacturer were 0.66 and 1 mmol/g for the PHO-CNF samples referred to as PHO-CNF$_{0.66}$ and PHO-CNF$_{1.00}$, respectively. The concentration of carboxylate groups in TO-CNF was 1 mmol/g. Uranyl acetate, Arsenazo III, ascorbic acid, perchloric acid, and nitric acid were all obtained from Sigma Aldrich. Milli-Q water (Millipore) was used for the preparation of all solutions.

Characterization of CNF

The electrostatic charge of CNF was determined with a Zetasizer Nano-ZS90 (Malvern), reported as zeta potential, and measured at pH 3, 5, 7, and 9 (adjusted by using 1 M HCl and NaOH) from 0.05 wt% CNF suspensions. The different types of CNF were imaged with a FEI Tecnai 12 TEM operating at 120 kV. For sample preparation, 3 μL of 0.01 wt% CNF suspension was drop casted on a copper grid with an ultrathin carbon support film and the excess solution was blotted with filter paper after 1 min of contact time, followed by drying under ambient conditions.

Thereafter, 3 μL of 2% uranyl acetate was drop casted onto the dried CNF sample in order to stain the sample. The excess solution was blotted with filter paper after 1 min of contact time, followed by drying under ambient conditions. FT-IR spectra of freeze-dried CNF samples were recorded with Nicolet 380 FT-IR Spectrometer using an ATR accessory. The spectra were recorded in the region of 400–4000 cm^{-1} with 0.5 cm^{-1} intervals.

Adsorption experiments

A dry mass of 5 mg of the respective nanocellulose and a total volume of 15 mL of solution were used in the adsorption experiments, unless otherwise mentioned. Experiments were conducted at room temperature (21–22 °C), which remained stable throughout the experiments. A stock solution of 2000 mg/L uranyl acetate was used to prepare the solutions. The adsorption isotherm studies were conducted with initial uranium concentrations of 10, 25, 50, 100, 200, 300, 400, and 500 mg/L. Experiments at different pH and with different CNF types were performed using an initial concentration of 100 mg/L uranium. For the isotherm study, for the comparison between CNF types, and for the selectivity study, the pH was adjusted to 6 using 2 M HCl and NaOH. In all experiments, glass vials were filled with 15 mL of the suspension containing uranium and CNF and sonicated to disperse the fibrils in an ultrasonic bath at 37 kHz for 5 min. The samples were then left in a shaker at 200 rpm for 55 min to reach the equilibrium. After the adsorption process, samples were taken from the solutions and filtered with 0.1 μm filters (Whatman). Samples without CNF having similar initial U(VI) concentrations were used as controls to analyze any possible adsorption of U(VI) onto the filters. Based on this analysis, the adsorption of uranium onto the filters was found to be negligible. Uranium concentrations were determined spectrophotometrically with Arsenazo III method (Khan et al. 2006) using a microplate reader (Synergy H1) to determine the absorbance of the solutions at 651 nm. Briefly, 25 μL of ascorbic acid (100 g/L), 175 μL of Arsenazo III (0.07 w/v% in 3 M perchloric acid) and 50 μL of sample were added to the wells of a microwell plate. If necessary, the samples were diluted to reach a maximum U(VI) concentration of 10 mg/L before mixing with ascorbic acid and Arsenazo III. For each

sample, two parallel measurements were conducted with the plate reader and the average of these values reported.

Selectivity experiments were conducted using a concentration of 10 mg/L for all the metals tested (U, Zn, Mn, and Cu). Other typical ions present in natural waters were also added to the solution according to Table S1 (adapted from Sankar et al. 2013). In the selectivity tests, two different amounts of PHO-CNF$_{1.00}$ were used, 5 mg and 0.25 mg (values given as dry mass in 15 mL solution). Metal concentrations in the samples used in the selectivity tests were analyzed with inductively coupled plasma mass spectrometry (ICP-MS) (PerkinElmer, NexION 300X). For ICP-MS analysis, the samples were diluted to a maximum concentration of 1 mg/L and digested with 5% (vol.) concentrated HNO$_3$ (68–70%) before analysis.

The percentage of U(VI) removed in adsorption studies was calculated based on Eq. (1):

$$U\ removal\ (\%) = \frac{C_0 - C_f}{C_0} \times 100\% \tag{1}$$

and the equilibrium adsorption capacities (q_e) were calculated using Eq. (2):

$$q_e = \frac{(C_0 - C_e)V}{m} \tag{2}$$

where C_0, C_f, and C_e are the initial, final and equilibrium concentrations (mg/L) of U(VI), respectively, V is the volume (L) and m is the mass of adsorbent (g) used.

Langmuir, Freundlich, and Sips isotherm models were used for fitting the experimental adsorption data. The Langmuir and Freundlich isotherm models are shown in Eqs. (3) and (4), respectively:

$$\frac{C_e}{q_e} = \frac{C_e}{q_{max}} + \frac{1}{q_{max}K_L} \tag{3}$$

$$\ln q_e = \ln K_F + \frac{1}{n}\ln C_e \tag{4}$$

where q_{max} is the maximum adsorption capacity (mg/g) and K_L is the Langmuir adsorption constant (L/mg). K_F is the Freundlich isotherm constant and n is the dimensionless heterogeneity factor.

The Sips isotherm model, a combination of the Langmuir and Freundlich isotherms, is expressed as Eq. (5):

$$\ln\left(\frac{q_e}{q_m - q_e}\right) = \frac{1}{n}\ln C_e + \ln K_s \tag{5}$$

where q_m is the maximum adsorption capacity (mg/g) and K_s is the median association constant.

Characterization of PHO-CNF$_{1.00}$ after adsorption

The uranium stock solution was diluted to reach final concentrations of 50, 100, 250, and 500 mg/L. After mixing with PHO-CNF$_{1.00}$, sonication and shaking as described earlier, a 10 μL drop of the PHO-CNF$_{1.00}$ uranium suspension was drop casted onto the carbon tape on aluminum stubs and the stubs were placed in a -80 °C freezer overnight and freeze dried at − 50 °C. For SEM imaging, the samples were sputter-coated with 3 nm of platinum-palladium and observed using an acceleration voltage of 1.6 kV with a scanning electron microscope (Zeiss Sigma VP). TEM samples for imaging after U(VI) adsorption were prepared by drop casting from the suspension with initial U(VI) concentration of 100 mg/L similarly as described in the characterization section without additional uranium staining.

X-ray photoelectron spectroscopy

Samples for XPS were prepared by vacuum filtration of PHO-CNF$_{1.00}$ onto 0.1 μm filters after adsorption of U(VI) from the initial concentrations of 0, 100 mg/L, and 500 mg/L. After vacuum filtration, the filter cakes were frozen at − 80 °C and freeze-dried to obtain dry films. An electron spectrometer (AXIS Ultra, Kratos Analytical, UK) with monochromatic Al Kα irradiation at 100 W under neutralization was used for the measurements. Three different spots from each film were scanned and elemental surface compositions of the films were determined from low resolution survey scans. High resolution measurements of uranium U 4f, carbon C1s and oxygen O1s were also conducted. Pure cellulose filter paper (Whatman) was used as an in situ reference in all measurements. Data analysis was performed with CasaXPS software, using fitting parameters customized for celluloses and the C–O component of the high resolution C1s at 286.7 eV as

the energy reference for all the spectra (Beamson and Briggs 1992; Johansson and Campbell 2004).

Uranium speciation

An ion speciation software (PHREEQC) was used to determine the uranyl speciation at pH range 3–7, and in the simulated drinking water used for selectivity experiments (Tables S2 and S3). The U(VI) concentration used for the calculations was 100 mg/L.

Results and discussion

Native and modified CNF

FT-IR was used to confirm the functional groups on the TO-CNF and PHO-CNF (Fig. 1a). The characteristic bands of cellulose were observed in all the samples (broad band at 3340 cm^{-1} due to O–H stretching vibrations, peak at around 1640 cm^{-1} corresponding to the O–H bending of adsorbed water and peaks at around 1030 and 2900 cm^{-1} corresponding to the C–O and C–H stretching vibrations, respectively). For the PHO-CNF samples, additional peaks were detected at around 820 cm^{-1}, 930 cm^{-1}, and 1230 cm^{-1} which are assigned to P–O–C, P–OH, and P=O stretching vibrations, respectively (Suflet et al. 2006). For the TO-CNF, a peak at around 1600 cm^{-1} was detected corresponding to the C=O

stretching vibration of the COO$^-$ group. The zeta potentials of all the CNFs were negative in the pH range tested (Fig. 1b). The zeta potential values for PHO-CNF and TO-CNF decreased as the pH increased. This can be explained by the deprotonation of carboxyl or phosphoryl groups. The zeta potentials of the native CNF indicate that it is negatively charged owing to the residual hemicelluloses (containing carboxyl groups) and other impurities originating from the fibers used to prepare the material.

TEM images of the CNFs used in the study are shown in Fig. 2. The images show a clear difference in the size of the native fibrils (Fig. 2a) compared to TO-CNF, PHO-CNF$_{0.66}$, and PHO-CNF$_{1.00}$ (Fig. 2b–d). The native CNF consists of long fibrils, while much shorter fibrils are present inTO-CNF and PHO-CNF, due to the chemical treatment used in the respective preparation.

Adsorption studies

Batch U(VI) adsorption experiments were conducted with the nanocelluloses. U(VI) adsorption was observed to happen within minutes but to ensure that equilibrium was reached, a contact time of 1 h was used in all adsorption tests.
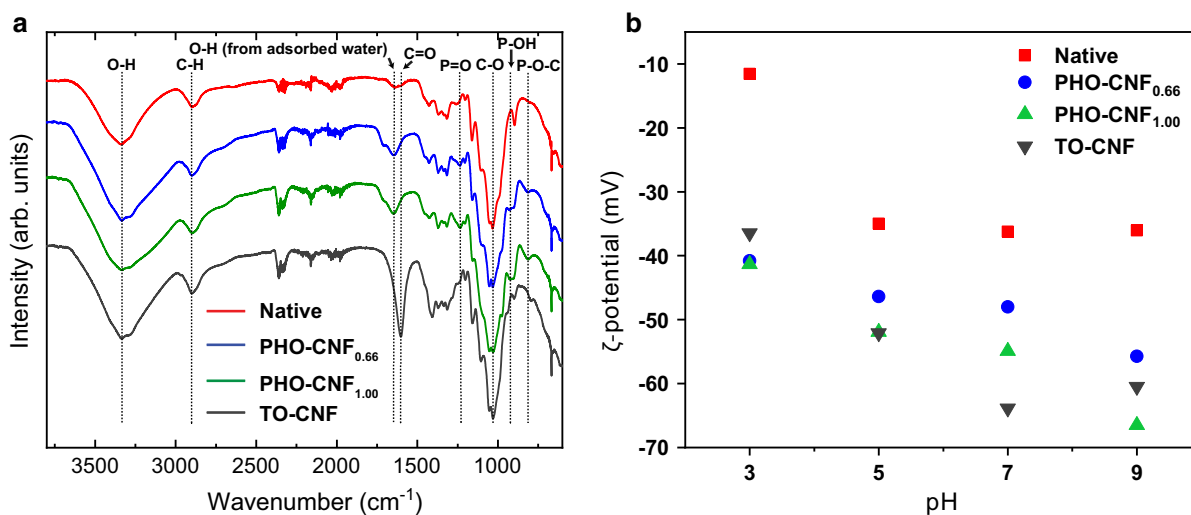

Fig. 1 a FT-IR spectra and b zeta potentials in the pH range 3–9 of native CNF, PHO-CNF$_{0.66}$, PHO-CNF$_{1.00}$, and TO-CNF
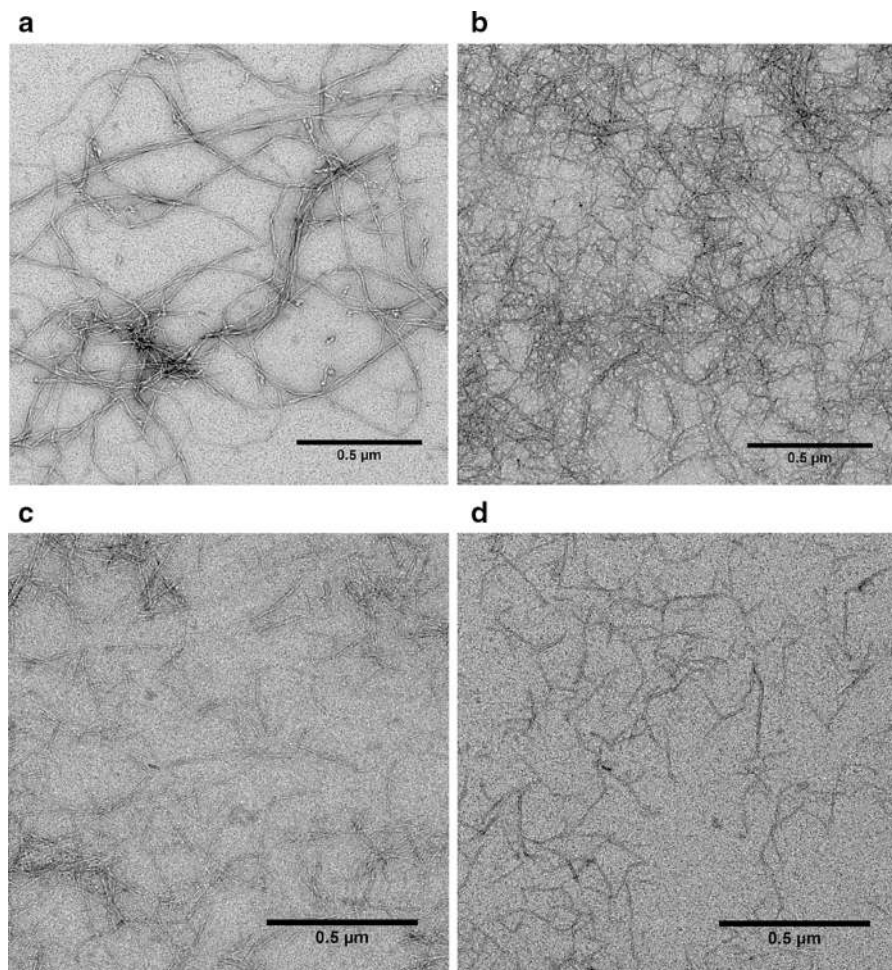
Fig. 2 TEM images of **a** Native CNF, **b** TO-CNF, **c** PHO-CNF$_{0.66}$, and **d** PHO-CNF$_{1.00}$

Comparison of adsorption on different types of CNF

First, the removal of U(VI) with the four different types of CNF was compared using an initial U(VI) concentration of 100 mg/L (Fig. 3). The results indicate that the PHO-CNF$_{1.00}$ was the most efficient of the nanocelluloses for uranium removal. The degree of phosphorylation was found to affect the removal of uranium only slightly, since 94% and 92% removal was observed with 1 mmol/g and 0.66 mmol/g phosphorylation degrees, respectively. However, the removal was significantly higher with PHO-CNF in comparison to TO-CNF (77%) or native CNF (7%). Based on the results, it can be concluded that the anionic charge of the CNF is an important factor in the adsorption of U(VI). The removal of U(VI) with PHO-CNF and TO-CNF can be mainly attributed to the
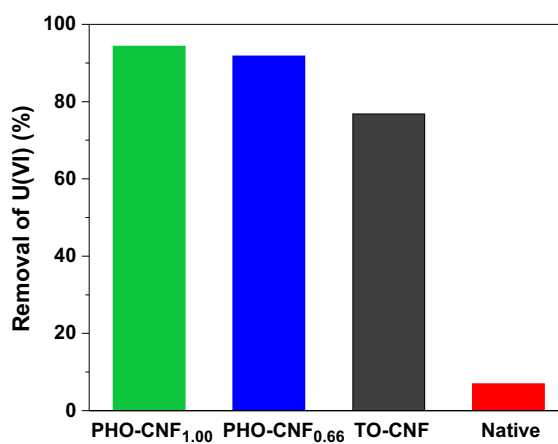

Fig. 3 Removal of U(VI) with PHO-CNF with varying degree of phosphorylation (1 mmol/g and 0.66 mmol/g), TEMPO oxidized CNF, and native fibrils

phosphoryl and carboxyl groups present on the fibrils. In the case of native CNF, the adsorption is most likely explained by the slight negative charge on the fibrils, as confirmed by the zeta potential measurements. However, the higher removal degree achieved with PHO-CNF compared to TO-CNF indicate the higher affinity between phosphoryl groups and U(VI). In addition, the smaller dimensions of the PHO-CNF and TO-CNF compared to native CNF lead to higher surface area, thus enabling higher adsorption capacities. Based on the results of the comparison study, adsorption tests were further continued with PHO-CNF$_{1.00}$.

Characterization of PHO-CNF$_{1.00}$ after adsorption

In batch adsorption experiments, we observed gelling of the nanocellulose at high initial uranium concentrations, e.g. 500 mg/L (Fig. S1). Thus, the interaction of the fibrils with U(VI) was studied by SEM imaging of the PHO-CNF$_{1.00}$ after adsorption using given initial U(VI) concentrations (Fig. 4). It can be observed that the adsorption at initial uranium concentrations of 50 and 100 mg/L did not affect the fibrillar morphology and thus the colloidal stability of PHO-CNF$_{1.00}$. However, an initial concentration of 250 mg/L led to the formation of sheet-like structures, and at 500 mg/L, also precipitate-like material was observed. In order to gain more insights on the formation of these structures, TEM images from samples that used an initial U(VI) concentration of 100 mg/L were taken after adsorption with PHO-CNF$_{1.00}$ (Fig. 5). The onset of aggregation can be observed in the images, as evidenced by the formation of fibril bundles, ultimately converging to sheet-like structures. It has been reported that due to the linear geometry of uranyl ion, sheet-like or chain-like structures can form upon complexation (Hu et al. 2018). The individual fibrils observed in the images were surprisingly uniform in width, indicating uniform coverage of phosphoryl groups which led to a spatially homogeneous adsorption of U(VI). Distinctively, the width of the fibrils was measured to be 15 ± 2 nm based on image analysis, which is larger than the width measured for the fibrils before adsorption (12 ± 2 nm).

These results indicate that crosslinking occurred between the fibrils and U(VI) at high initial U(VI) concentrations, which leads to aggregation of the fibrils. A similar gelling effect has been reported for

CNF containing anionic functional groups and reports are available on the hydrogelation of carboxylated CNF with monovalent (Ag^+) (Dong et al. 2013a), divalent (Ca^{2+}, Zn^{2+}, Cu^{2+}), and trivalent cations (Al^{3+} and Fe^{3+}) (Dong et al. 2013b). Gelation was suspected to initiate from the screening of repulsive charges caused by cation-carboxylate interactions (Dong et al. 2013b). Moreover, UO_2^{2+} has been found to cause the gelation of TO-CNF. 150 mg/L was reported as the threshold concentration of UO_2^{2+} for gel formation in a 0.05 wt% CNF suspension (Ma et al. 2012). Formation of gels through ionic cross-linking has also been reported with TO-CNF and Al^{3+} cations (Masruchin et al. 2015). In this study, the gelling effect is likely due to the reduction of electrostatic repulsion between the nanofibers after the adsorption of U(VI).

Results of XPS analysis of PHO-CNF$_{1.00}$ after U(VI) adsorption (Fig. 6 and Table S4) confirmed the presence of uranium in its hexavalent state on the fibers, based on the position of the U4f$_{7/2}$ peak (382.5 ± 0.5 eV) which was detected after adsorption from both 100 mg/L and 500 mg/L samples (Moulder et al. 1995). The XPS results are summarized in Table 1, where the amounts of phosphorous, sodium, and uranium were calculated in relation to the nominal surface cellulose content of the respective sample, in order to remove the effect of adventitious carbon from the results. The nominal surface cellulose content was calculated from the total carbon and the C–O component of C1s. The decrease in surface cellulose upon increasing uranium content is mainly due to the increase of adventitious carbon (Fig. 6 inset, C–C peak at 285 eV), indicating changes in the surface energy of cellulose surfaces (Johansson et al. 2011) upon uranium adsorption.

The amount of sodium, which is present as a counterion of phosphoryl groups in the PHO-CNF, was found to decrease as the amount of uranium increased, indicating the occurrence of ion exchange. The amount of phosphorous remained stable in 0 mg/L and 100 mg/L samples, and decreased slightly in the 500 mg/L sample. This is likely due to the increased coverage of uranium on the PHO-CNF$_{1.00}$. High-resolution spectra of O 1s and U 4f with superimposed spectra from 100 to 500 mg/L samples are shown in Fig. S2. The similar shape of the superimposed U 4f spectra of 100 and 500 mg/L samples clearly indicates that uranium was adsorbed in both cases in a similar chemical form.
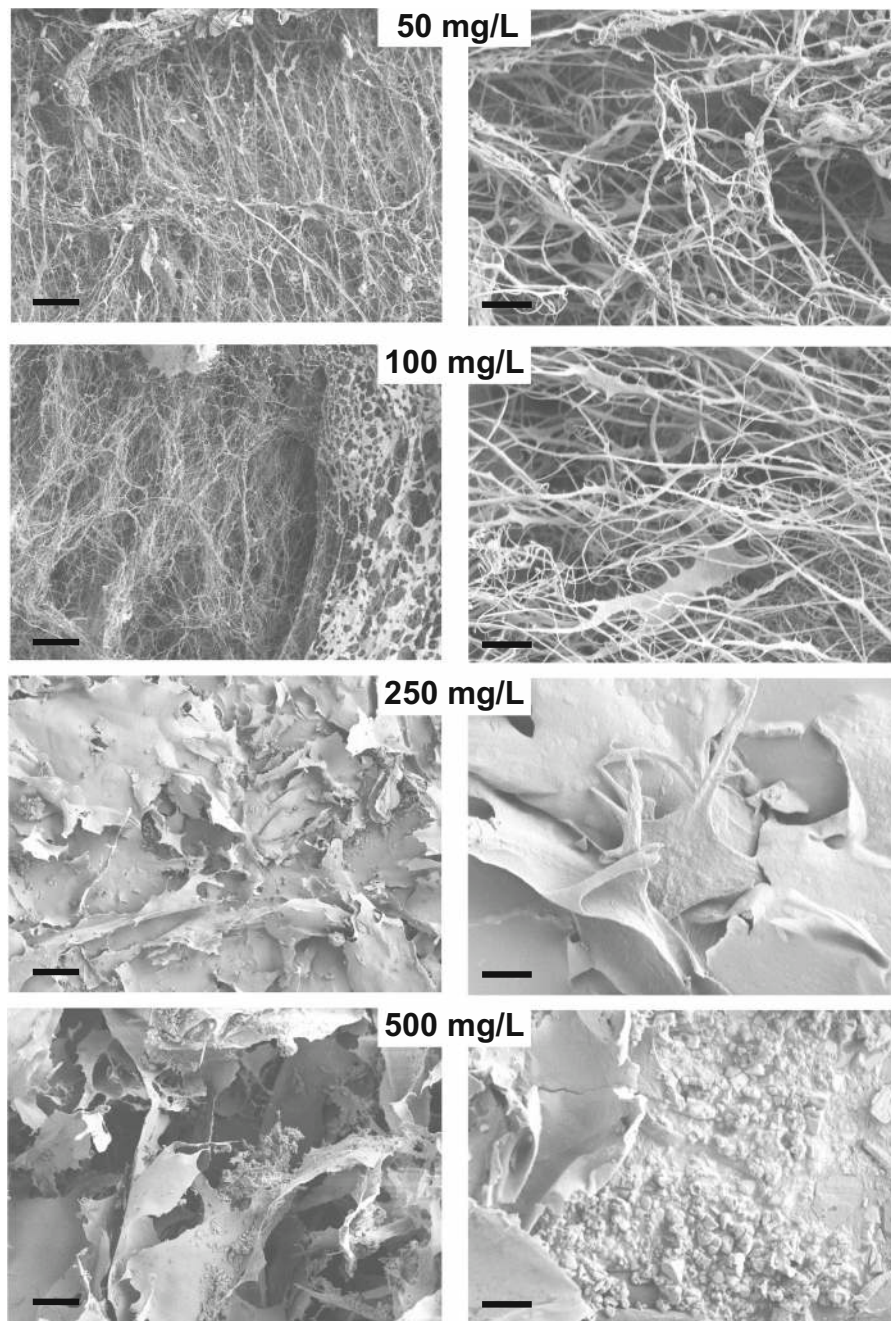
Fig. 4 SEM images of PHO-CNF$_{1.00}$ after 1 h contact with solutions with initial U(VI) concentration of 50, 100, 250, and 500 mg/L. Scale bars are 20 μm (left) and 3 μm (right)

Apart from elemental information within the topmost few nanometers, XPS survey spectra also yield information on elemental depth distributions within the surface region (Tougaard 1998; Johansson et al. 2004). According to the background shapes of carbon, oxygen, and uranium (see Fig. 6 and Fig. S2), it is clear that uranium species observed in both treated samples were present as islands or open films with similar thicknesses (at least 3–5 nm).
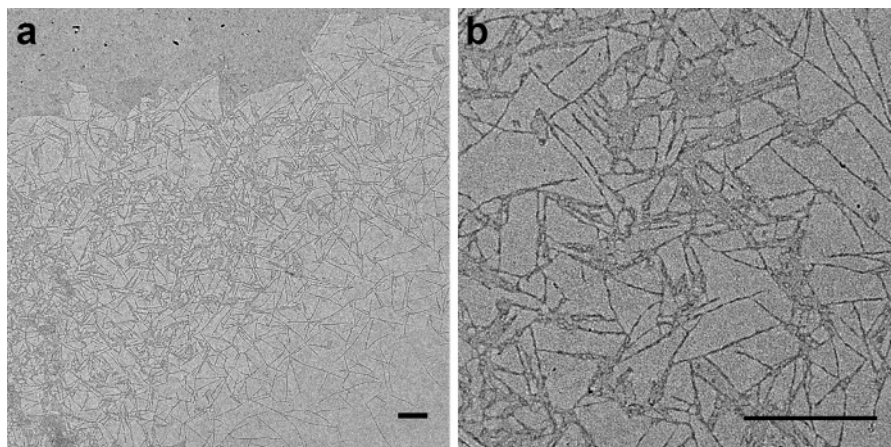
Fig. 5 TEM images showing **a** overview and **b** magnified view of PHO-CNF$_{1.00}$ after adsorption of U(VI) from initial U(VI) concentration of 100 mg/L. The scale bars correspond to 1 μm
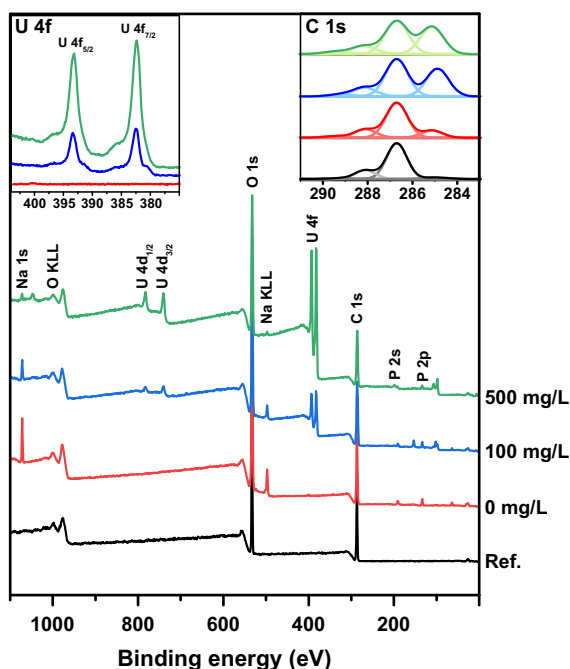

Fig. 6 Survey spectra from XPS measurements of PHO-CNF$_{1.00}$ after U(VI) adsorption from initial concentrations of 0, 100, and 500 mg/L and the in situ cellulose reference sample. High-resolution U 4f and C 1s spectra are included in the insets, as indicated

Effect of pH on U(VI) adsorption

Both the adsorbent charge and the speciation of U(VI) are influenced by pH (Guo et al. 2018). The optimum pH for heavy metal adsorption is typically acidic, around 4–6. At around neutral pH and higher, heavy

metals often tend to precipitate into hydroxides (Hokkanen et al. 2014). The removal of uranium did not vary significantly in the pH range 3–6, as shown in Fig. 7. However, when pH was increased to 7, a ∼ 30% reduction in the uranium removal was observed. UO_2^{2+} speciation is dependent on pH, temperature and composition of the water. At pH values below 5, uranium mainly exists as UO_2^{2+} in solution. At pH values between 5–7, neutral and anionic uranium species can also form in addition to cationic uranyl complexes (Aly and Hamza 2013). At pH >6 , UO_2^{2+} forms complexes in the presence of carbonate causing reduction in U(VI) removal as reported for nanocrystalline titanium dioxide (Wazne et al. 2006) and iron oxyhydroxide (Wazne et al. 2003).

Adsorption capacity

In order to quantify the maximum adsorption capacity of PHO-NFC$_{1.00}$, adsorption experiments were performed with varying initial U(VI) concentration. The results were fitted to the Langmuir, Freundlich, and Sips adsorption isotherm models (Fig. 8). As expected, the adsorbed uranium amount increases with the equilibrium concentration (C_e) and eventually stabilizes at high C_e values. Table S5 shows the isotherm parameters calculated based on Eqs. (3), (4), and (5). Based on the R^2 values, the Sips isotherm was found to fit best with the experimental data. This model is, in fact, a combination of the Langmuir and Freundlich isotherms. The Langmuir isotherm

Table 1 Summary of XPS results

Sample	Nominal surface cellulose content (%)	P (at%) in relation to cellulose content (%)	Na (at%) in relation to cellulose content (%)	U (at%) in relation to cellulose content (%)
Reference Whatman paper	98	0.0	0.0	0.0
0 mg/L	77	4.1	3.2	0.0
100 mg/L	60	4.1	1.9	2.0
500 mg/L	57	3.3	0.6	6.8
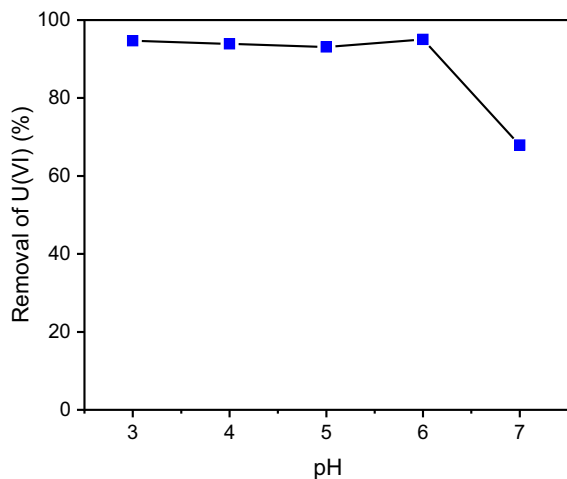
Fig. 7 Effect of pH on U(VI) removal with PHO-CNF$_{1.00}$

assumes monolayer adsorption with a homogeneous surface while the Freundlich isotherm takes into account multilayer adsorption on heterogeneous surfaces (Lombardo and Thielemans 2019). However, in practical terms, the isotherm models do not fully reveal the actual mechanisms of adsorption.

Table 2 presents q_{max} values of uranium for adsorbents based on different cellulose nanomaterials or phosphorylated biomaterials. Typical maximum adsorption capacities reported for uranium are between 100 and 1000 mg/g. In addition to the high selectivity of the phosphoryl groups to U(VI), the high adsorption capacity achieved in this study is attributed to the high surface area provided by the nanosized fibrils and surface charge density of the PHO-CNF$_{1.00}$.

An estimation of the theoretical maximum adsorption capacity of PHO-CNF$_{1.00}$ at pH 6 can be made assuming that all the U(VI) in the solution occurs as $(UO_2)_3(OH)_5^+$ species. This is reasonable since according to the speciation analysis presented in Table S2,

96% of the uranium is in this form. Considering a coordination ratio of 2:1 between this species and phosphoryl groups, the maximum adsorption capacity of the PHO-CNF$_{1.00}$ is calculated to be 1430 mg/g, which is very close to the value derived from the Sips isotherm based on the experimental data (1550 mg/g). Taken any uncertainty on the speciation and the exact form of adsorbed uranium, the results indicate extensive capturing of uranium by PHO-CNF.

Selectivity

Figure 9 shows the selectivity of PHO-CNF$_{1.00}$ to U(VI) compared to selected divalent metals (Cu, Zn, and Mn) in the presence of other ions typically present in natural waters (Table S1). The removal percentages were found to be in the order of U > Cu > Zn > Mn with 5 mg PHO-CNF$_{1.00}$, corresponding to a metal/adsorbent weight ratio of 0.03. When the amount of CNF was decreased, at a metal/adsorbent weight ratio of 0.6, the selectivity of the PHO-CNF$_{1.00}$ to U(VI) is clearly demonstrated. The results also indicate that high removal rates for uranium could be achieved with PHO-CNF$_{1.00}$ in the presence of competing divalent ions at similar concentrations. Another interesting observation from the results is that the removal of U(VI) increased from 95 to 99% in the presence of competing ions when the initial uranium concentration was 10 mg/L. A similar result has been reported for uranium removal by magnesium ferrite loaded carbon nanosheets (Li et al. 2019). The removal percentage achieved here is comparable to the high removal efficiency reported for uranyl acetate using an amyloid-carbon membrane (99.35%) (Bolisetty and Mezzenga 2016).

The selectivity of PHO-CNF$_{1.00}$ to U(VI) can be explained by the high affinity of the phosphoryl groups
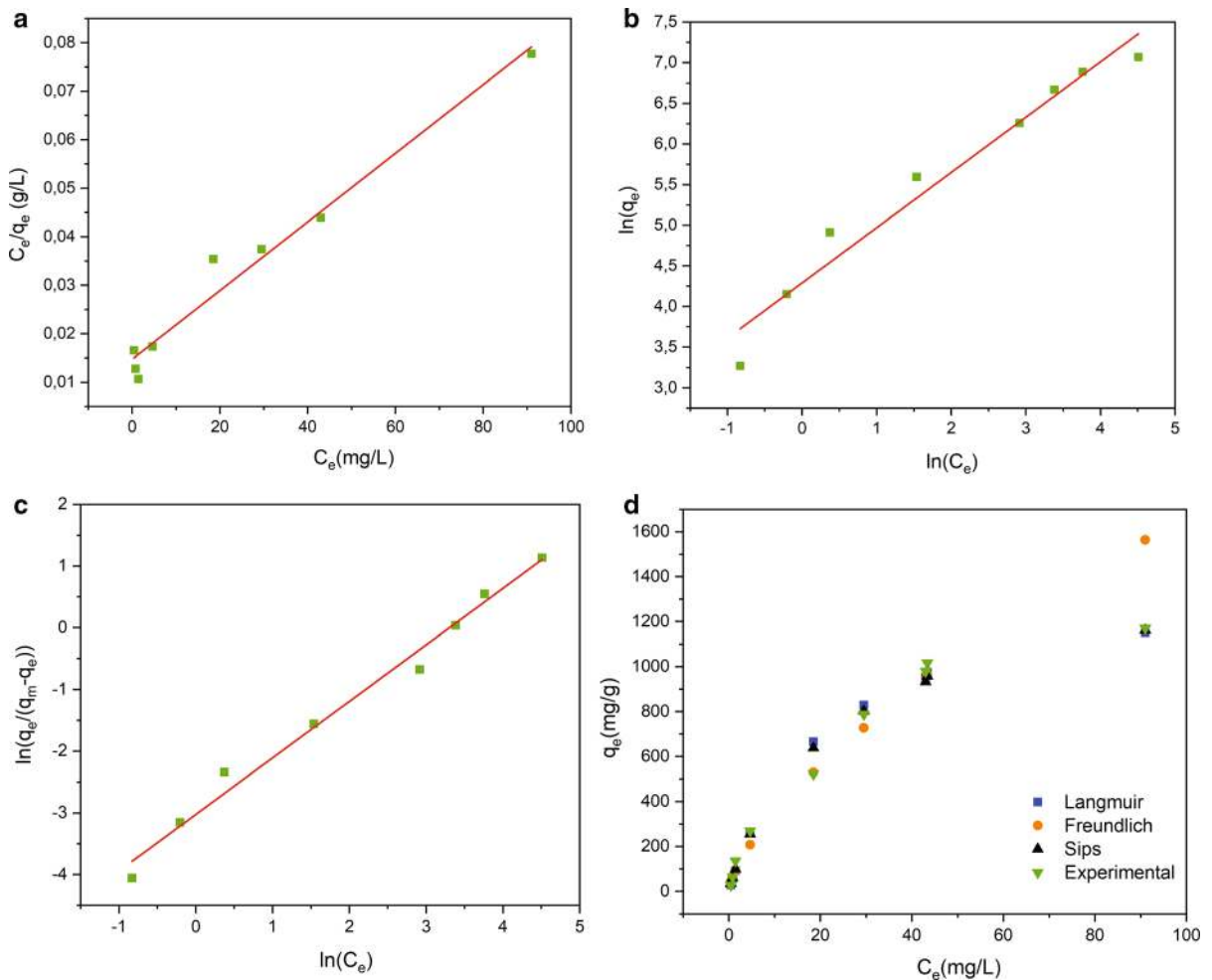
Fig. 8 Effect of initial concentration of U(VI) on adsorption. Adsorption data fitted to **a** Langmuir isotherm, **b** Freundlich isotherm, and **c** Sips isotherm. **d** Adsorption data for PHO-CNF$_{1.00}$ compared to the theoretical Langmuir, Freundlich, and Sips isotherm models

Table 2 Maximum adsorption capacity of uranium on different organic adsorbents

Adsorbent	q_{max} (mg/g)	References
TEMPO CNF	167 (at pH 6.5)	Ma et al. (2012)
Phosphorylated cactus fibers	107 (at pH 4.5)	Prodromou and Pashalidis (2013)
Phosphorylated chitosan	55 (pH not reported)	Morsy (2015)
Carboxycellulose nanofibers	1467 (at pH 7)	Sharma et al. (2017)
Phosphorylated GO-chitosan	779 (at pH 5)	Cai et al. (2017)
Phosphorylated chitosan CMC	978 (at pH 5)	Cai et al. (2019)
Phosphorylated CNF	1550 (at pH 6)	This work

to uranium. Based on the XPS and batch adsorption studies, it is proposed that the phosphoryl groups play a significant role in the adsorption process. Other factors that can contribute to the high selectivity are the high oxidation state, charge-to-radius ratio and the likelihood of U(VI) to hydrolyze, since solid surfaces typically have a higher affinity to the hydrolyzed species (Cai et al. 2019). Mesoporous silica with phosphonic groups has been found to have high selectivity to uranium against interfering elements
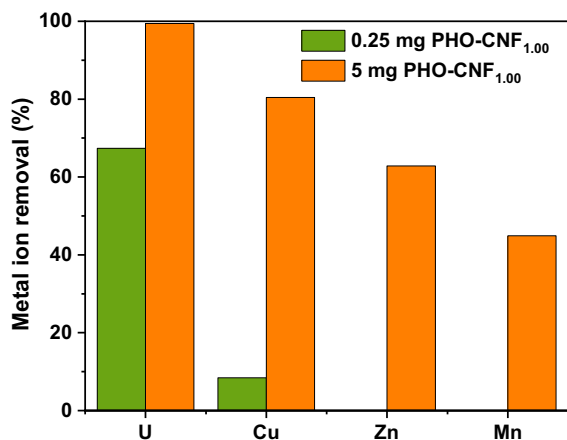
Fig. 9 Selectivity of PHO-CNF$_{1.00}$ to U(VI). Removal of heavy metals by PHO-CNF$_{1.00}$ was studied from solutions containing U, Cu, Zn, and Mn (initial concentrations were 10 mg/L)

such as As, K Ni, Mo, Cu, and Pb (Sarafraz et al. 2017). High selectivity of phosphate-functionalized polyethylene towards uranium compared to Cu^{2+}, Al^{3+}, Fe^{3+}, and V^{4+} has also been reported (Shao et al. 2017).

Conclusions

This work demonstrates that PHO-CNF can efficiently remove U(VI) from aqueous solutions with an unprecedented maximum bioadsorption capacity of 1550 mg/g. Over 90% removal of U(VI) was achieved in a pH range of 3–6. The efficiency of PHO-CNF can be attributed to the high surface area, anionic charge and the affinity of the phosphoryl groups to U(VI). The morphology of the substrates was studied after adsorption by SEM, TEM, and XPS, which indicated that U(VI) forms sheet-like aggregates with PHO-CNF at high initial U(VI) concentrations. The high selectivity of the PHO-CNF against other metals and ions present in natural waters is demonstrated, which is critical in application of the material for U(VI) removal. Overall, this study shows that PHO-NFC has great potential as an environmentally friendly bioadsorbent for U(VI) removal from highly contaminated waters.

References

Aly MM, Hamza MF (2013) A review: studies on uranium removal using different techniques: overview. J Disper Sci Technol 34:182–213. https://doi.org/10.1080/01932691.2012.657954

Asikainen A, Kahlos H (1979) Anomalously high concentrations of uranium, radium and radon in water from drilled wells in the Helsinki region. Geochim Cosmochim Acta 43:1681–1686. https://doi.org/10.1016/0016-7037(79)90187-X

Beamson G, Briggs D (1992) High resolution XPS of organic polymers. In: The Scienta ESCA 300 Database. Wiley, Chichester, p 56

Berto S, Crea F, Daniele PG, Gianguzza A, Pettignano A, Sammartano S (2012) Advances in the investigation of dioxouranium(VI) complexes of interest for natural fluids. Coordin Chem Rev 256:63–81. https://doi.org/10.1016/j.ccr.2011.08.015

Bethke K, Palantöken S, Andrei V, Roß M, Raghuwanshi VS, Kettemann F, Greis K, Ingber TTK, Stückrath JB, Valiyaveettil S, Rademann K (2018) Functionalized cellulose for water purification, antimicrobial applications, and sensors. Adv Funct Mater 28(1800409):1–14. https://doi.org/10.1002/adfm.201800409

Bolisetty S, Mezzenga R (2016) Amyloid-carbon hybrid membranes for universal water purification. Nat Nanotechnol 11:365–372. https://doi.org/10.1038/NNANO.2015.310

Božič M, Liu P, Mathew AP, Kokol V (2014) Enzymatic phosphorylation of cellulose nanofibers to new highly-ions adsorbing, flame-retardant and hydroxyapatite-growth induced natural nanoparticles. Cellulose 21:2713–2726. https://doi.org/10.1007/s10570-014-0281-8

Bykov GL, Ershov BG (2009) Sorption of uranyl ions on phosphorylated lignin. Radiochemistry 51:292–294. https://doi.org/10.1134/S1066362209030138

Cai Y, Wu C, Liu Z, Zhang L, Chen L, Wang J, Wang X, Yang S, Wang S (2017) Fabrication of a phosphorylated graphene oxide-chitosan composite for highly effective and selective capture of U(VI). Environ Sci Nano 4:1876–1886. https://doi.org/10.1039/c7en00412e

Cai Y, Chen L, Yang S, Xu L, Qin H, Liu Z, Chen L, Wang X, Wang S (2019) Rational synthesis of novel phosphorylated chitosan-carboxymethyl cellulose composite for highly effective decontamination of U(VI). ACS Sustain Chem Eng 7:5393–5403. https://doi.org/10.1021/acssuschemeng.8b06416

Chen H, Wang Y, Zhao W, Xiong G, Cao X, Dai Y, Le Z, Zhang Z, Liu Y (2017) Phosphorylation of graphehe oxide to improve adsorption of U(VI) from aquaeous solutions. J Radioanal Nucl Chem 313:175–189. https://doi.org/10.1007/s10967-017-5274-2

Dong H, Snyder JF, Tran DT, Leadore JL (2013a) Hydrogel, aerogel and film of cellulose nanofibrils functionalized with silver nanoparticles. Carbohydr Polym 95:760–767. https://doi.org/10.1016/j.carbpol.2013.03.041

Dong H, Snyder JF, Williams KS, Andzelm JW (2013b) Cation-induced hydrogels of cellulose nano fibrils with tunable moduli. Biomacromolecules 14:3338–3345. https://doi.org/10.1021/bm400993f

Ghasemi Torkabad M, Keshtkar AR, Safdari SJ (2017) Comparison of polyethersulfone and polyamide nanofiltration membranes for uranium removal from aqueous solution. Prog Nucl Energy 94:93–100. https://doi.org/10.1016/j.pnucene.2016.10.005

Guo X, Feng Y, Ma L, Yu J, Jing J, Gao D, Khan AS, Gong H, Zhang Y (2018) Uranyl ion adsorption studies on synthesized phosphoryl functionalised MWCNTs: a mechanistic approach. J Radioanal Nucl Chem 316:397–409. https://doi.org/10.1007/s10967-018-5761-0

Hokkanen S, Repo E, Suopajärvi T, Liimatainen H, Niinimaa J, Sillanpää M (2014) Adsorption of Ni(II), Cu(II) and Cd(II) from aqueous solutions by amino modified nanostructured microfibrillated cellulose. Cellulose 21:1471–1487. https://doi.org/10.1007/s10570-014-0240-4

Hu F, Di Z, Lin P, Huang P, Wu M, Jiang F, Hong M (2018) An anionic uranium-base metal-organic framework with ultralarge nanocages for selective dye adsorption. Cryst Gowth Des 18:576–580. https://doi.org/10.1021/acs.cgd.7b01525

Johansson L-S, Campbell J (2004) Reproducible XPS on biopolymers: cellulose studies. Surf Int Anal 36:1018–1022. https://doi.org/10.1002/sia.1827

Johansson L-S, Campbell J, Koljonen K, Kleen M, Buchert J (2004) On surface distributions in natural cellulosic fibres. Surf Int Anal 36:706–710. https://doi.org/10.1002/sia.1741

Johansson L-S, Tammelin T, Campbell JM, Setälä H, Österberg M (2011) Experimental evidence on medium driven cellulose surface adaptation demonstrated using nanofibrillated cellulose. Soft Matter 7:10917–10924. https://doi.org/10.1039/C1SM06073B

Kapnisti M, Noli F, Misaelides P, Vourlias G, Karfaridis D, Hatzidimitriou A (2018) Enhanced sorption capacities for lead and uranium using titanium phosphates; sorption, kinetics, equilibrium studies and mechanism implication. Chem Eng J 342:184–195. https://doi.org/10.1016/j.cej.2018.02.066

Khan MH, Warwick P, Evans N (2006) Spectrophotometric determination of uranium with arsenazo-III in perchloric acid. Chemosphere 63:1165–1169. https://doi.org/10.1016/j.chemosphere.2005.09.060

Klemm D, Cranston ED, Fischer D, Gama M, Kedzior SA, Kralisch D, Kramer F, Kondo T, Lindström T, Nietzsche S, Petzold-Welcke K, Rauchfuß F (2018) Nanocellulose as a natural source for groundbreaking applications in materials science: today's state. Mater Today 21:720–748. https://doi.org/10.1016/j.mattod.2018.02.001

Li X, Li Y, Wu Q, Zhang M, Guo X, Li X, Ma L, Li S (2019) Ultrahigh uranium uptake by magnetic magnesium ferrite loaded hydrothermal carbon nanosheets under acidic condition. Chem Eng J 365:70–79. https://doi.org/10.1016/j.cej.2019.02.002

Liu P, Borrell PF, Božič M, Kokol V, Oksman K, Mathew AJ (2015a) Nanocelluloses and their phosphorylated derivatives for selective adsorption of Ag^+, Cu^{2+} and Fe^{3+} from industrial effluents. J Hazard Mater 294:177–185. https://doi.org/10.1016/j.jhazmat.2015.04.001

Liu X, Li J, Wang X, Chen C, Wang X (2015b) High performance of phosphate-functionalized graphene oxide for the selective adsorption of U(VI) from acidic solution. J Nucl Mater 466:56–64. https://doi.org/10.1016/j.jnucmat.2015.07.027

Lombardo S, Thielemans W (2019) Thermodynamics of adsorption on nanocellulose surfaces. Cellulose 26:249–279. https://doi.org/10.1007/s10570-018-02239-2

Ma H, Hsiao BS, Chu B (2012) Ultrafine cellulose nanofibers as efficient adsorbents for removal of UO_2^{2+} in water. ACS Macro Lett 1:213–216. https://doi.org/10.1021/mz200047q

Masruchin N, Park B, Causin V, Um IC (2015) Characteristics of TEMPO-oxidized cellulose fibril-based hydrogels induced by cationic ions and their properties. Cellulose 22:1993–2010. https://doi.org/10.1007/s10570-015-0624-0

Mautner A, Maples HA, Kobkeatthawin T, Kokol V, Karim Z, Li K, Bismarck A (2016) Phosphorylated nanocellulose papers for copper adsorption from aqueous solutions. Int J Environ Sci Technol 13:1861–1872. https://doi.org/10.1007/s13762-016-1026-z

Morsy AMA (2015) Adsorptive removal of uranium ions from liquid waste solutions by phosphorylated chitosan. Environ Technol Innov 4:299–310. https://doi.org/10.1016/j.eti.2015.10.002

Moulder JF, Stickle WF, Sobol PE, Bomben KD (1995) Handbook of X-ray photoelectron spectroscopy: a reference book of standard spectra for identification and interpretation of XPS data. Perkin-Elmer Corp., Physical Electronics Division, Eden Prairie

Prodromou M, Pashalidis I (2013) Uranium adsorption by non-treated and chemically modified cactus fibres in aqueous solutions. J Radioanal Nucl Chem 298:1587–1595. https://doi.org/10.1007/s10967-013-2565-0

Rajala S, Siponkoski T, Sarlin E, Mettänen M, Vuoriluoto M, Pammo A, Juuti J, Rojas OJ, Franssila S, Tuukkanen S (2016) Cellulose nanofibril film as a piezoelectric sensor

material. ACS Appl Mater Interfaces 8:15607–15614. https://doi.org/10.1021/acsami.6b03597

Riegel M, Schlitt V (2017) Sorption dynamics of uranium onto anion exchangers. Water 9(268):1–17. https://doi.org/10.3390/w9040268

Sakaguchi T, Horikoshi T, Nakajima A (1981) Adsorption of uranium by chitin phosphate and chitosan phosphate. Agric Biol Chem 45:2191–2195. https://doi.org/10.1080/00021369.1981.10864862

Sankar MU, Aigal S, Maliyekkal SM, Chaudhary A, Anshup KA, Chaudhari K, Pradeep T (2013) Biopolymer-reinforced synthetic granular nanocomposites for affordable point-of-use water purification. Proc Natl Acad Sci 110:8459–8464. https://doi.org/10.1073/pnas.1220222110

Sarafraz H, Minuchehr A, Alahyarizadeh G, Rahimi Z (2017) Synthesis of enhanced phosphonic functional groups mesoporous silica for uranium selective adsorption from aqueous solutions. Sci Rep 7:1–12. https://doi.org/10.1038/s41598-017-11993-5

Shao D, Li Y, Wang X, Hu S, Wen J, Xiong J, Asiri AM, Marwani HM (2017) Phosphate-functionalized polyethylene with high adsorption of uranium(VI). ACS Omega 2:3267–3275. https://doi.org/10.1021/acsomega.7b00375

Sharma PR, Chattopadhyay A, Sharma SK, Hsiao BS (2017) Efficient removal of UO_2^{2+} from water using carboxycellulose nanofibers prepared by the nitro-oxidation method. Ind Eng Chem Res 56:13885–13893. https://doi.org/10.1021/acs.iecr.7b03659

Sirviö JA, Hasa T, Leiviskä T, Liimatainen H, Hormi O (2016) Bisphosphonate nanocellulose in the removal of vanadium(V) from water. Cellulose 23:689–697. https://doi.org/10.1007/s10570-015-0819-4

Su S, Liu Q, Liu J, Zhang H, Li R, Jing X, Wang J (2018) Functionalized sugarcane bagasse for U(VI) adsorption from acid and alkaline conditions. Sci Rep 8:1–10. https://doi.org/10.1038/s41598-017-18698-9

Suflet DM, Chitanu GC, Popa VI (2006) Phosphorylation of polysaccharides: new results on synthesis and characterisation of phosphorylated cellulose. React Funct Polym 66:1240–1249. https://doi.org/10.1016/j.reactfunctpolym.2006.03.006

Sylwester ER, Hudson EA, Allen PG (2000) The structure of uranium(VI) sorption complexes on silica, alumina, and montmorillonite. Geochim Cosmochim Acta 64:2431–2438. https://doi.org/10.1016/S0016-7037(00)00376-8

Tougaard S (1998) Accuracy of the non-destructive surface nanostructure quantification technique based on analysis of the XPS or AES peak shape. Surf Int Anal 24:249–269. https://doi.org/10.1002/(SICI)1096-9918(199804)26:4<249::AID-SIA368>3.0.CO;2-A

Um W, Mattigod S, Serne RJ, Fryxell GE, Kim DH, Troyer LD (2007) Synthesis of nanoporous zirconium oxophosphate and application for removal of U(VI). Water Res 41:3217–3226. https://doi.org/10.1016/j.watres.2007.05.030

Voisin H, Bergström L, Liu P, Mathew AP (2017) Nanocellulose-based materials for water purification. Nanomaterials 7:57. https://doi.org/10.3390/nano7030057

Wazne M, Korfiatis GP, Meng X (2003) Carbonate effects on hexavalent uranium adsorption by iron oxyhydroxide. Environ Sci Technol 37:3619–3624. https://doi.org/10.1021/es034166m

Wazne M, Meng X, Korfiatis GP, Christodoulatos C (2006) Carbonate effects on hexavalent uranium removal from water by nanocrystalline titanium dioxide. J Hazard Mater 136:47–52. https://doi.org/10.1016/j.jhazmat.2005.11.010

World Health Organization WHO (2011) Guidelines for drinking-water quality, 4th edn

Xie Y, Chen C, Ren X, Wang X, Wang H, Wang X (2019) Emerging natural and tailored materials for uranium-contaminated water treatment and environmental remediation. Prog Mater Sci 103:180–234. https://doi.org/10.1016/j.pmatsci.2019.01.005

Xue G, Feng Y, Ma L, Gao D, Jing J, Yu J, Sun H, Gong H, Zhang Y (2017) Phosphoryl functionalized mesoporous silica for uranium adsorption. Appl Surf Sci 402:53–60. https://doi.org/10.1016/j.apsusc.2017.01.050

Yu XF, Liu YH, Zhou ZW, Xiong GX, Cao XH, Li M, Zhang ZB (2014) Adsorptive removal of U(VI) from aqueous solution by hydrothermal carbon spheres with phosphate group. J Radioanal Nucl Chem 300:1235–1244. https://doi.org/10.1007/s10967-014-3081-6

Zhou L, Huang Z, Luo T, Jia Y, Liu Z, Adesina AA (2015) Biosorption of uranium(VI) from aqueous solution using phosphate-modified pine wood sawdust. J Radioanal Nucl Chem 303:1917–1925. https://doi.org/10.1007/s10967-014-3725-6